Chasing the Green Flash: a Global Illumination Solution for Inhomogeneous Media

D. Gutierrez
University of Zaragoza
diegog@unizar.es

F.J. Seron
University of Zaragoza
seron@unizar.es

O. Anson
University of Zaragoza
oanson@ivo.cps.unizar.es

A. Muñoz
University of Zaragoza
orbananos@able.es

Abstract

Several natural phenomena, such as mirages or the green flash, are owed to inhomogeneous media in which the index of refraction is not constant. This makes the light rays travel a curved path while going through those media. One way to simulate global illumination in inhomogeneous media is to use a curved ray tracing algorithm, but this approach presents some problems that still need to be solved. This paper introduces a full solution to the global illumination problem, based on what we have called curved photon mapping, that can be used to simulate several natural atmospheric phenomena. We also present a model of the Human Visual System (HVS) to display images in a more realistic way, taking into account how we perceive luminances in a real-world scene. This is of special interest in the green flash effect, where some of the perceived green is owed to bleaching of the photoreceptors in the human eye.

Keywords: Rendering, global illumination, photon mapping, natural phenomena, inhomogeneous media, realism.

1 Introduction

Several of the atmospheric effects we see in nature, from mirages to the green flash, are owed to light traveling curved paths [Minnaert 1993], and therefore are impossible or exceedingly costly to simulate with synthetic imagery using standard Monte Carlo ray tracing techniques. Nevertheless, modeling of nature has been one of the most ambitious goals of the Computer Graphics community.

Most ray tracing algorithms are based on the assumption that light rays travel following a straight path. This is so because mentioned algorithms consider only homogeneous media, where properties are kept constant. While this assumption works well for a great number of situations, it nevertheless imposes several restrictions on the scenes and effects that can be reproduced, including some of the phenomena that occur in our atmosphere.

Most of the media are in fact inhomogeneous to one degree or another, with properties varying continuously from point to point. The atmosphere, for instance, is in fact inhomogeneous since pressure, temperature and other properties do vary from point to point, and therefore its optic characterization, given by the index of refraction, is not constant.

A light ray propagating in a straight line would then be accurate only in two situations: either there is no media through which the light travels (as in outer space, for instance), or the media are homogeneous. But with inhomogeneous media, new phenomena occur. For instance, light in warm air (which has a lower optical density) moves faster than in cold air, which is denser.

According to Fermat's Principle, light crossing a medium gets curved towards the areas with the greater index of refraction. This index of refraction, which defines the optical characteristics of the medium, is a function of both humidity and density, as well as wavelength, with density being a function of pressure and temperature itself. Therefore, in a medium where temperature changes continually, so will the direction of propagation, thus making light rays travel curved paths (with the degree of curvature being a function of wavelength).

2 State of the art

There are several examples that simulate the behaviour of light in the atmosphere, such as the works of Musgrave [1993] or Nishita [1998]. There is also some previous work on curved ray tracing in inhomogeneous media. Berger and Trout [1990] recreate mirages by subdividing the medium into various homogeneous layers, with a different index of refraction for each one. Musgrave [1990] proposes a purely reflective model as the means of forming mirages, while Groeller [1995] uses sources of nonlinearity such as gravity centers, gravity lines, chaotic systems and parametric curved rays. Stam and Languenou [1996] propose a solution by obtaining the differential equation that describes the trajectory of the ray from the equation of the light wave. Finally, Serón et al. [2002] describe a more general method, free of the restrictions that appear in the above papers regarding the dependences of the index of refraction, and propose a partial solution to the problem using the general equation, based on Fermat's

principle, that describes the phenomenon. None of these works, though, can successfully follow the complete light paths: from the lights through inhomogeneous media to interaction with geometry, through inhomogeneous media again before finally reaching the eye. The basic problem of following all these paths is explained in the next section.

This paper describes a global illumination solution based on what the authors call curved photon mapping techniques. The basic algorithm is explained in the next section. Section 3 describes an atmosphere profile manager to set up the scenes according to the phenomenon that needs to be simulated. The algorithm is validated through several test images in Section 4, while Section 5 presents the green flash and our work on the Human Visual System and the bleaching of photoreceptors in the eye. The results are shown in Section 6, and the future work is discussed in Section 7.

3 Curved photon mapping

Traditionally, light travelling trough inhomogeneous media has been simulated by using ray tracing techniques [Glassner 1989]. Basically, in backward ray tracing, a ray is shot from the eye into the scene until it reaches an object, and from that intersection point more rays are shot towards the lights to find the color of the corresponding pixel.

This works well for homogeneous media, where the light rays travel in a straight path. But the situation changes when using curved ray tracing: curving the eye ray until it reaches an object in the scene is conceptually simple. We do not know where each ray is going to end up after being curved by the medium, but we do not care either, since it will eventually hit some object or be lost in infinity, just as with straight ray tracing. The problem arises when shooting additional rays from the intersection point to the lights. Even though we know both the start and end points of the ray, it is difficult to find a curve that passes through those two points while also obeying the nonlinearity caused by the inhomogeneous medium. Just shooting rays hoping one will eventually hit the light is obviously very ineffective. This is a problem similar to computing caustics by using path tracing or any other backward ray tracing method. Caustics are concentrated light reflections on diffuse surfaces caused by refraction through transparent surfaces, and to simulate them in the image it would be necessary to trace a random ray from a diffuse surface, and have the ray interact with several specular surfaces and then hit the light. Arvo [1986] first introduced forward ray tracing to simulate caustics, while bidirectional path tracing [Lafortune and Willems 1996; Veach and Guibas 1994] combines both backward and forward ray tracing by generating some path vertices starting from the light sources and some from the eye.

However, all these techniques would fail again (or be too computationally expensive) in an inhomogeneous media. Shooting rays from the objects to the eye in forward ray tracing, or obtaining shadow rays in bidirectional path tracing would face the same basic problem as with backward ray tracing: to find a curve that passes through two given points while obeying the nonlinearities of the medium.

Groeller [1995] proposes several solutions to this problem: the first one supposes that the light rays are only curved from the eye to the intersection point, but travel in a straight line from the intersection point to the light source. The second solution consists in assigning color to the intersection point regardless of the light sources, for instance by using textures with the illumination already pre-calculated. These are obvious simplifications that will work well for general image synthesis, but do not reflect the physics of the system. The second solution is in fact used in [Serón et al. 2002], since the authors concentrated mainly on solving the general equation accurately. Another idea is to voxelize the space and get the approximate direction of incoming light by shooting light rays through the voxels from each light, saving the results in a pre-computed structure. As far as the authors know, there is not much more literature regarding this problem.

Since neither a pure backward, forward nor bi-directional ray tracing solution seems viable for inhomogeneous media where rays get curved, we sought a combined approach, creating a rendering environment named Lucifer, based on photon mapping techniques.

Photon mapping is a two-pass algorithm [Jensen 2001]. In the first pass photons are shot from each light into the scene, and traced as they interact with the geometry. In each collision, the Russian Roulette algorithm decides whether each photon is absorbed, reflected or transmitted. When the photon hits a diffuse material, it is stored. The data structure that stores all these photons is called the photon map. The second pass consists on a modified ray tracing algorithm, but instead of shooting shadow rays, radiance is estimated from the nearest stored photons around the intersection point. Specular reflections are obtained by standard ray tracing, since the probabilities of a photon being reflected in the exact specular direction towards the eye are infinitesimal.

The photon mapping algorithm allows a full global illumination simulation, including color bleeding and caustic generation. As we are going to see, it can also be adapted to inhomogeneous media, by calculating the curved trajectory of the photons during the photon tracing phase. This adaptation is what we refer to as curved photon mapping.

3.1 Trajectory of the photons

The main forte of Lucifer is its capability of providing a full global illumination solution in inhomogeneous media, by accurately curving both photons and eye rays as they travel through the medium. As a starting point to obtain this curved trajectory of the photons, we take Fermat's principle [Glassner 1995], which can be formulated as "light, in going between two points, traverses the route *l* having the smallest optical path

length *L*". The optical path *L* is defined as the index of refraction times the traveled path. In its differential form, it can be written as *dL=ndl*. According to Fermat's principle, the optical path along a light ray trajectory must be a minimum, therefore δL =0, where δL is given by:

$$\delta L = \delta \int_A^B ndl = \int_A^B \delta n\, dl + \int_A^B n\delta(dl) = \int_A^B \frac{\partial n}{\partial x_i}\delta x_i dl + \int_A^B n\delta(dl)$$

(Eq. 3.1)

where x_i are the components of *l*. Given that $dl^2 = dx^2 + dy^2 + dz^2$, considering dx_i as variables and taking increments we get $\delta(dl) = \frac{dx_i}{dl}\delta(dx_i)$ so that equation 3.1 results:

$$\int_A^B n\delta(dl) = n\frac{dx_i}{dl}\delta x_i \Big]_A^B - \int_A^B \delta x_i \frac{d}{dl}\left(n\frac{dx_i}{dl}\right)dl$$

(Eq. 3.2)

Since the different considered trajectories start in the fixed points *A* and *B*, $\delta x_i(A) = 0$ and $\delta x_i(B) = 0$, so equation 3.2 results as follows:

$$\delta L = \int_A^B \left[\frac{\partial n}{\partial x_i} - \frac{d}{dl}\left(n\frac{dx_i}{dl}\right)\right]\delta x_i dl = 0$$

(Eq. 3.3)

This equation must be true for any value of δx_i, which lets us come up with the equation to obtain the trajectory of a light ray in an inhomogeneous medium with a known index of refraction, which is:

$$\frac{d}{dl}\left(n\frac{d\vec{r}}{dl}\right) - \nabla n = 0 \leftrightarrow \frac{d}{dl}\left(n\frac{dx_j}{dl}\right) - \frac{\partial n}{\partial x_j} = 0 \quad \text{(j=1,2,3)}$$

(Eq. 3.4)

where *l* is the length of the arc, *n* is the index of refraction of the medium and $\vec{r} = x_j$ with (j=1,2,3) are the coordinates of the point. If the index of refraction is known for every point of the medium, we first calculate that index and the slope of the curve at step *i,* advance Δl_i along the direction of the tangent to reach step *i+1*, and calculate the new index of refraction and tangent again. To calculate the direction of the tangent we first obtain a numerical approximation by discretizing the equation, effectively replacing differentials by increments. We then apply the Richardson's extrapolation algorithm to select an optimal integration step for each instant, given an estimate of the tolerable error. The process ends when we get to the intersection point of the photon with an object, and gets started again if the Russian Roulette algorithm does not absorb the photon at the surface.

Two maps are used in the current version of this technique: a caustics photon map, to represent caustics in a more efficient way using projection maps, and a second photon map to represent both direct and indirect illumination, excluding caustics. We have named this second map the diffuse photon map.

As a simple test scene we use a closed, square room with a cross-shaped window in the left wall. A strong spotlight is placed outside looking inside, so that most of its light enters the room through the cross-shaped widow. Figure 3.1, left, shows the resulting illumination when there is an extremely hot layer right below the ceiling of the room. This makes the index of refraction inside the room a function of height, thus creating an inhomogeneous media. Photon paths and rays are curved according to equation 3.4. The resulting curved photon map can be seen in figure 3.1, right.

The image was rendered at a 400x300 resolution, shooting 3.000.000 photons from the spotlight and using 150 photons for estimating the irradiance. It took 4'47'' on a P-III @800Mhz and 512Gb of RAM, owed to the time needed to calculate the curved paths. The error threshold when using Richardson's extrapolation algorithm was set to 0.01.

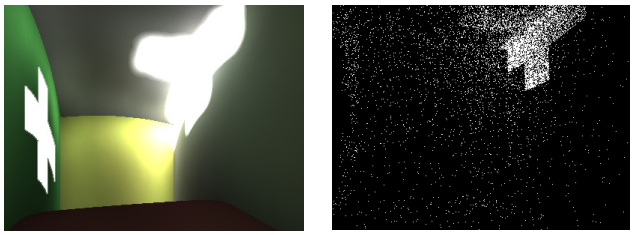

Figure 3.1: Test scene for the curved photon mapping algorithm. Left: resulting illumination. Right: the curved photon map used

4 Atmosphere profile manager

As we have said, the atmosphere is an inhomogeneous medium with changing parameters, like temperature or pressure. This is what causes some of its optical effects, such as mirages or the green flash, and it is also the reason why they can be seen only under certain, very specific conditions. In order to simulate some of these phenomena, we then need to have a model of the atmosphere that is versatile enough to be adapted specifically for a desired effect.

Our approach to obtain an atmospheric profile is based upon the USA Standard Atmosphere. It defines the pressure and temperature at different heights, through empirical graphs and tables. In order to obtain useful results to apply Fermat's principle, a continuous function is needed, as opposed to discrete data. We then obtain a function through linear interpolation. The possibility of using some other kind of interpolation (maybe quadratic) is being considered, because some numeric methods to solve differential equations need not only the function to be continuous but also its derivative [Burden and Douglas Faires 1995].

Once we have an atmosphere profile, its density is obtained directly from temperature and pressure using the Perfect Gas Law [Bruton 1996]:

$$\rho = \frac{PM}{RT}$$

(Eq. 4.1)

where ρ is the density we want to obtain, *T* is the temperature, *P* is the pressure, *M* is the mean mass of

the molecules of a mixed atmosphere ($28.96 \cdot 10^{-3}$ kg/mol typically) and R is the gas constant, 8.314510 J/mol·K.
To include the fact that the index of refraction is also a function of wavelength, we use Cauchy's formula [Born and Wolf 2002]:

$$n(\lambda) = a \cdot (1 + \frac{b}{\lambda^2}) + 1$$

(Eq 4.2)

where a and b are constants which depend on the medium. In case of air $a = 28{,}79 \cdot 10^{-5}$ and $b = 5{,}67 \cdot 10^{-5}$. The Sellmeier's approximation could also be used instead [Born and Wolf 2002].
Now we have on the one hand density as a function of temperature and pressure (which are a function of height themselves using the USA Standard Atmosphere) and on the other hand the index of refraction as a function of wavelength (equation 4.2). To obtain the refraction index at any height and any wavelength we should combine both functions. We can do so by applying the Glastone-Dale principle, which says that refractivity (refraction index minus 1) is proportional to the density:

$$n(h, \lambda) = \rho(h) \cdot (n(\lambda) - 1) + 1$$

(Eq. 4.3)

All the steps which have lead to equation 4.3 have been based so far on the USA Standard Atmosphere, which does not provide the special atmospheric conditions under which some phenomena can be seen. Any desired condition, though, can be reproduced if instead of taking the initial pressure and temperature values from the USA Standard Atmosphere we use the specific pressure and temperature conditions that lead to the phenomenon we want to reproduce, which can usually be found in the literature.
In order to simulate the desired phenomena we need to modify this Standard Atmosphere, obtaining modified atmosphere profiles from initial parameters such as inversion layers [van der Werf et al. 2003]. To achieve this, we have created an atmosphere profile manager, from where inversion layers can be appended to any given profile (usually the standard) by the following analytical function, known as the Fermi distribution:

$$T(h, x) = T_{ATM}(h) - \Delta T(x) + \frac{\Delta T(x)}{1 + e^{-\frac{h - h_{ciso}(x)}{a(x)}}}$$

(Eq. 4.4)

where x is the distance in the direction parallel to the Earth's surface, $h_{ciso}(x)$ is the height of the inversion layer about which the added temperature profile is centered, $\Delta T(x)$ is the temperature jump across the inversion and the diffuseness parameter $a(x)$ determines the width of the jump.

5 Validation of the method

To validate our approach this far we have designed several scenes, aimed at mimicking some well-known or spectacular atmospheric effects, the green flash amongst them. Photons were not used in these images to light the scene. They were designed mainly to test both our method of resolution of the curved trajectories and our atmosphere profile manager. We used simple geometry combined with textures taken from real pictures, but the sizes of the objects (sun, Earth…) and the atmosphere data are taken from the real world, in order not to fake the effect. We consider the properties of the atmosphere to be independent of x, since the changes in that coordinate are usually small and can be neglected. Considering a gradient also in that direction would enable us to simulate some other phenomena, like the Novaya Zemlya effect [van der Werf et al. 2003].

5.1 Mirages

There are two types of mirages: inferior and superior. The inferior mirage occurs when there is a decrease of temperature with increasing height. As a consequence, the rays approaching the ground are curved upwards, generating an inverted image of the object in the ground. Since the mirage image appears under the location of the real object, the effect is known as inferior mirage. This can typically happen when an asphalt road has been overheated by the sun rays. The ground heated by an intense solar radiation causes a pronounced heating of the air layers near the ground. As a consequence of that temperature gradient, the index of refraction increases with height and the rays become curved towards the region in which the index of refraction is greater. Figure 5.1 shows an inferior mirage on the road near the horizon. This has been obtained by making the index of refraction in a particular portion of the road lower than the rest, an effect caused by a local heating of the air above the road.

Figure 5.1: Inferior mirage on the road.

Superior mirages occur when the temperature increases as the height increases, which causes the light rays to

Figure 5.2: Simulated sunset effects and their real counterparts (flattened sun, split sun and double sun).

be bent downwards. The image appears above the position of the real object, therefore the effect is known as superior mirage. These type of mirages happen usually at sea, when the water is colder than the air above it.

5.2 Sunset effects

Other interesting refraction phenomena occur during sunsets. The flattened sun is probably the most common one, and happens when the atmosphere has an index of refraction that decreases with height. It is so common because usually the density of the air decreases as one moves away from the Earth, and so the index of refraction decreases as well. As a result of this, the sun is not seen as a perfect circle, but appears rather flattened along the vertical axis. The rays become curved downwards, towards the areas with a greater index of refraction, causing the distortion of the sun. Moreover, the sun appears to be higher than it really is.

The split sun is a curious phenomenon that may happen when there is a cold air layer near the earth and a warmer layer above it. The phenomenon of total reflection may take place when a ray passes from one medium to another with a smaller index of refraction with an adequate angle. In that situation there is no refracted ray, and the ray is reflected. This configuration causes the split sun effect, with two portions of the sun separated by an empty strip located around the horizontal plane that passes through the observer.

The double sun phenomenon takes place when there is a very thin layer of warm air over the surface of the earth. In this case, the rays traced from the observer that do not make contact with the ground are not affected by the warm layer and therefore the sun is perceived without distortion. However, the rays which do make contact with the warm layer become curved upwards. As a consequence, part of them intersects again with the sun, thus causing the double image of the sun.

Figure 5.2 shows several images of the simulated sunset effects, along with their real-world counterparts. The difference between the simulated double sun effect and the real one is owed to the thickness of the warm layer and the position of the sun relative to the observer. Different combinations of these two parameters will give different images based on the same double-sun effect.

6 The green flash

So far, dispersion has not been taken into account for the mirages and sunsets simulations, since its effect in the phenomena is negligible. However, every refraction phenomenon includes a certain degree of dispersion, and some atmospheric refraction phenomena provoke a greater dispersion of light, and the green flash is arguably the most spectacular of them all. As our first step towards a complete simulation of the effect, we are going to reproduce the so-called academic green flash, an effect that occurs even in a Standard Atmosphere, taking refraction as a function of wavelength.

The green flash is a very transitory effect, lasting only a few seconds. When the sun is setting, and therefore it is low on the horizon, the path that the light rays travel is longer. Since the atmosphere is denser below than above, the light rays are bent downwards, but because of the index of refraction being a function of wavelength the blue-green rays are bent more than the red ones. The result is that we see a blue-green rim on

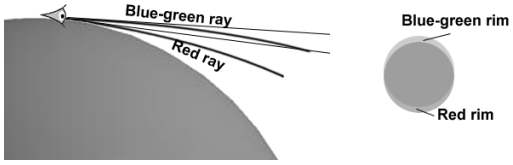

Figure 6.1: Sketch of the green flash

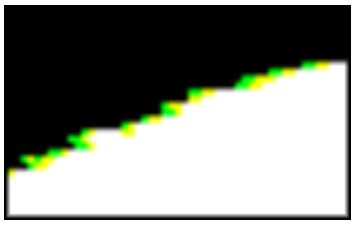

Figure 6.3: Close up of the academic green flash

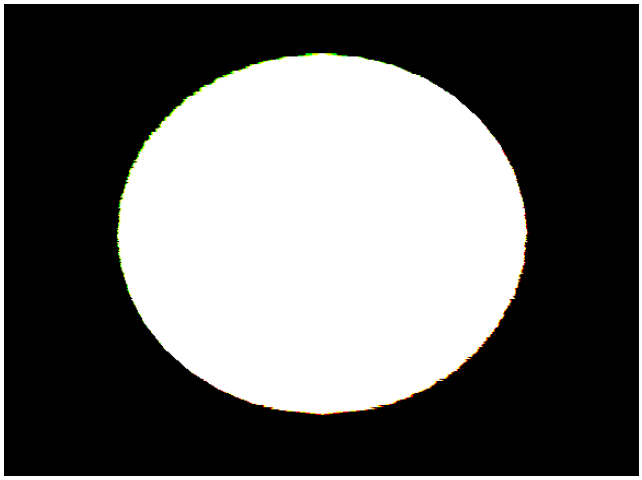

Figure 6.2: The academic green flash

top of the solar disc, and a red rim at the bottom (see figure 6.1). Aerosol extinction and Rayleigh scattering [Preetham 2003] eliminate most of the blue from the top rim, thus making the green purer. The red rim at the bottom is usually below the line of horizon and cannot be usually seen, but the effect is nevertheless known as the red flash. Figure 6.2 shows the simulation of the green flash; there is a tiny green rim on the upper half of the solar disk, and a tiny red one on the bottom side, just as expected. The solar disk has been artificially kept white and the background black to help perceive the effect in the images. A close-up of the picture allows us to better distinguish the green on top of the solar disk (Figure 6.3). As the images show, the Standard Atmosphere by itself produces a green flash about ten times smaller than the eye can actually see. It can only be seen by the naked eye when specific special atmospheric conditions that deviate from the standard occur, creating mirages that magnify its appearance.

6.1 The human visual system: bleaching

What makes the green flash specially interesting, from a Computer Graphics point of view, is the fact that not only is the effect caused by the wavelength dependency of the index of refraction (as opposed to the mirages and sunsets presented before), but it is magnified by the human visual system as well, through a process known as bleaching. This means that, in order to simulate it properly, we need both a correct global illumination algorithm for inhomogeneous media (validated in Section 4), and a model of the human observer that takes bleaching into account.

The human eye can undergo a loss of spectral sensitivity at moderate and high light intensities which is referred to as bleaching. When waiting for the green flash to occur, the retina has been exposed to very bright red light for relatively a long time. That bleaches some of the red-sensitive photopigments in the L cones (the long wavelength cones). The amount of degenerated pigment (more precisely, a protein known as rhodopsin) is proportional to the luminous intensity received by the pigment. As more pigment is bleached, the effective pigment density decreases and the spectral sensitivity becomes narrower, although the wavelength of peak sensitivity is unchanged. This degeneration has a great effect on our spectral sensitivity, and the now less sensitive cones will perceive red as yellow, and yellow as green. The effect has been previously studied in the field of Computer Graphics by [Pattanaik et al. 2000], based on the model of color vision of [Hunt 1995].

In the rods, the effects of bleaching on spectral sensitivity are insignificant; instead, very small changes on rhodopsin density provoke very large adaptive changes in rod sensitivity. This is usually a short term effect, but exposure to very high levels, especially to the shorter wavelengths, can lead to permanent vision loss, including blindness.

In cones, on the other hand, the effects of bleaching on pigment concentration can have large effects on spectral sensitivity and may need to be taken into account when evaluating chromatic adaptation and color matching.

Formulae are available for calculating the amount of photopigment bleached for both long (equilibrium) and short duration bleaching conditions. They rely on knowing the half constant of bleaching: the intensity for which the percentage of bleached and unbleached pigment is 50 percent. Estimates of this half bleaching constant have been determined from fundamental reflectometry for the rods [Rushton 1972] and for the combined M (medium wavelength) and L cones [Rushton and Henry 1968]. Separate estimates of the half bleaching constant of the M cones [Rushton 1963] and of the L cones [Rushton 1965] have also been

obtained, but they do not seem to be very accurate. A reliable estimate of the constant of the S (short wavelength) cones has not been obtained yet, although it is known that the S cones may be sensitive to photopic damage, even at moderate levels of blue light [Harwert and Sperling 1971; Harwert and Sperling 1975; Sperling 1986].

Several studies have been completed to obtain the half bleaching constant. According to [Rushton 1965], the long wavelength photopigment is half bleached at retinal illuminance levels (amount of energy entering the human eye) of 4.89 log trolands (td) in a ten-second exposure, or at 3.8 log td in the steady state. Other studies come up with 4.6 and 4.3 log td respectively, and suggest that a value of 6.1 log td (20.000 td) be adopted [Geisler 1978; Geisler 1979].

However, such values are based on adaptation to white or yellow lights that bleach both M and L cones, so a light that bleached just one class of cone would need to be only half as bright (10.000 td). In the case of setting sun, where most of the energy reaching the eye falls in the long wavelength side of the spectrum, the half bleaching constant for the L cones will therefore be close to 4 log td [Walraven 1981]. We will use that value for our simulation, since it also falls within the ranges proposed by the studies mentioned.

As we have seen, retinal illuminances are expressed in trolands, computed by multiplying the scene luminance by the effective eye pupil area. Larger pupils admit more light. When the scene luminance is very low, the diameter of the pupil can be as large as 7 mm, while at very high luminances it may be as small as 2 mm. A good relationship between pupil diameter and scene luminance is the equation recommended by [Wyszecki 1982] (eq. 6.1).

$$\log d = 0.8558 - 0.000401 \cdot (\log L + 8.6)^3$$

(Eq. 6.1)

The effective pupil area for estimating retinal luminance is less than the actual pupil area because the relative contribution of light to the sensation of brightness decreases as the light enters the pupil at increasing distance from the center of the pupil. This is called the Stiles-Crawford effect [Smith 1988]. It is a phenomenon of cone (or photopic) vision and does not occur for rod (or scotopic) vision. It is thought to be due to cone geometry. The ratio between effective and actual pupil area is called the effectivity ratio, a quantity that varies with pupil diameter and takes into account the Stiles-Crawford effect. The effective pupil area is thus the actual pupil area times this ratio R, expressed in the eq. 6.2.

$$R = 1 - 1.06 \cdot 10^{-2} \cdot d^2 + 4.19 \cdot 10^{-5} \cdot d^4$$

(Eq. 6.2)

where d is pupil diameter in mm. Estimated retinal luminance I (eq. 6.1, expressed in trolands), taking R, the pupil area and the scene luminance L into account, is:

$$I = R \times pupil\ area\ \left(in\ mm^2\right) \times L\ \left(in\ cd/m^2\right)$$

(Eq. 6.1)

Having obtained I plus the half bleaching constant, the following equation may be used to approximate the effect of bleaching in the stationary state [cvision.ucsd.edu]:

$$1 - p = \frac{I}{I + I_0}$$

(Eq. 6.2)

where p is the percentage of unbleached pigment; I is the intensity of bleaching light, in trolands; I_0 is the half bleaching constant , also in trolands.

Now we need to know how this bleaching of the L cones affects perception. To do so, we can use functions obtained from [Cornsweet 1970], that relate the perception threshold with the proportion of pigment in bleached state (see figure 6.1). Bleaching the rhodopsin by one percent raises this threshold by ten (decreases sensitivity by ten). Figure 6.1 shows how bleaching 50 percent of the rhodopsin in the rods raises the threshold by 10 log units while the same 50-percent bleaching of cone photopigment raises the threshold by just about one and a half log units. Therefore, rod sensitivity is not fully accounted for at the receptor level and may be explained by further retinal processing. It can be seen that the bleaching of cone photopigment has a smaller effect on cone thresholds.

Figure 6.2, left, shows the result of applying this model of bleaching to the image shown in Figure 6.2: all the yellow pixels have turned to green, producing a thicker green rim. For the reader to better appreciate the effect on printed paper, we have also added an image indicating the pixels of the original image that have been made greener by the bleaching algorithm (Figure 6.2, right).

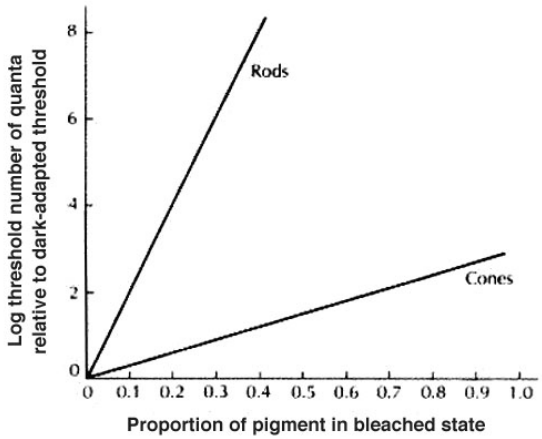

Figure 6.1: relation between perception threshold and bleached pigment (after [webvision.med.utah.edu])

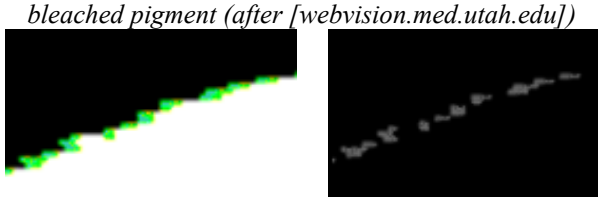

Figure 6.2: Left: Close up of the green flash with the bleaching algorithm applied. Right: Green pixels enhanced by bleaching

6.2 S·E·K·E·R

To correctly display the images calculated in Lucifer, we then feed them into S·E·K·E·R. This standalone application runs a tone reproduction algorithm that maps images from real, calculated luminances to final display luminances, while simulating several mechanisms of the human visual system.
This application is based on the work of [Ward et al. 1997]. S·E·K·E·R generates the adaptation luminances histogram of the HDR image and modifies it to discover clusters of adaptation levels. Afterwards, human visual limitation models are applied to simulate the effects of the human visual system. Finally the image is mapped to match the human contrast sensitivity.
We have followed two criteria to do a reliable tone reproduction: on the one hand, it preserves visibility. That means that an object can be seen in the image if and only if it can be seen in the real scene. On the other hand, the image must induce the same subjective sensation in the observer as if she were watching the real scene. The algorithm reproduces the sensation of brightness, the visual acuity, contrast and color perception, including the bleaching effect explained above, that makes the computed green flash greener.

7 Results

Our approach to obtain a full global illumination solution in inhomogeneous media is based on exploiting the independency in the photon map algorithm between light propagation (photon casting and tracing, first pass) and visibility determination (ray tracing, second pass). This idea is implemented by the curved photon-mapping algorithm. It works the same way than the standard photon-mapping algorithm, but it can handle inhomogeneous media as well by using Fermat's principle and solving equation 3.4 to obtain curved paths.
It is then also a two-pass algorithm: first, the path of each emitted photon is curved as it is being traced throughout the scene, using equation 3.4. Storing the photons (which paths have now been curved) on diffuse surfaces follows the same process as though the photons had not been curved.
During the second pass, the rays traced from the eye are also curved using again equation 3.4. To account for direct illumination, no shadow rays are shot towards the lights as in the original photon mapping algorithm; instead, radiance is estimated by using the diffuse photon map. This way, we avoid having to find the curved shadow ray that links the intersection point and the light while obeying the nonlinearities of the medium. We obtain the index of refraction as a function of wavelength from standard pressure and height data, thus enabling us to simulate dispersion effects.
We ensure the correctness of the method by using Fermat's principle to calculate the curved trajectories of the photons, generating several test images that simulate mirages, sunsets and the green flash to also validate the visual results. The atmosphere profile manager lets us create the different scenarios rather quickly.
Finally, we have presented S·E·K·E·R, our standalone, tone reproduction application that includes a model of the human visual system. More specifically, the model of bleaching is being used in the simulation the elusive green flash.

8 Future work

The results obtained so far show the viability of the approach. As the system gets refined over time, we nevertheless plan to generate better images that mimic some more complex natural phenomena, such as ducting or the Novaya Zemlya effect [van der Werf et al. 2003].
The green flash model obtained this far is purely academic, referred to by some authors as "the textbook green flash" [Young 2000]. A more complete model will be developed, taking into account also the mirages that help magnify its effect in the real world.
We also plan to extend this work with volume curved photon maps, to simulate other effects involving participating media, computing both elastic and inelastic scattering. Possible areas of interest are underwater imagery or driving simulators where the effects of fog need to be accounted for while testing visibility.
Finally, given the fact that finding all the curved paths of both photons and rays is computationally very expensive, optimization strategies are specially important. Another line of future work to reduce the rendering times implies the parallelization of the code to be run on a Beowulf system.

Figure 8.1: A picture of the green flash

Acknowledgements

This research was partly done under the sponsorship of the Spanish Ministry of Education and Research

through the projects TIC-2000-0426-P4-02 and TIC-2001-2392-C03-02.

References

ARVO , J.. 1986. Backward ray tracing, in *Developments in ray tracing, ACM SIGGRAPH '86* Seminar Notes, volume 12.

BERGER, M. and TROUT , T. 1990. Ray tracing mirages, *IEEE Computer Graphics and Applications, 11(5)*, may 1990, 36-41.

BORN, M. and WOLF, E. *Principles of Optics: Electromagnetic Theory of Propagation, Interference and Diffraction of Light.* Cambridge University Press, ISBN 0-521-642221, 2002.

BRUTON, D. 1996 *Optical determination of atmospheric temperature profiles,* submitted to the Office of Graduate Studies of Texas A&M University, 1996.

BURDEN, R. L. and DOUGLAS FAIRES J. 1995. *Numerical Analysis* PWS, Boston, USA.

CORNSWEET, T.N. 1970. *Visual Perception*. New York. Academic Press.

http://cvision.ucsd.edu

HARWERT, R.S. and SPERLING, H.B. 1971. Prolonged color blindness induced by intense spectral light in reshus monkeys. *Science*, 174, 520-523.

HARWERT, R.S. and SPERLING, H.B. 1975. Effects of intense visible radiation on the increment threshold spectral sensitivity of the rhesus monkey eye. *Vision Research*, 15, 1193-1204.HUNT, R.W.G. 1995 *The reproduction of colour*, Chapter 31. Fountain Press, England.

JENSEN, H. W. 2001. *Realistic image synthesis using photon mapping*, AK Peters, ISBN 1-56881-147-0.

LAFORTUNE , E. P. and WILLEMS, Y. D. 1993. Bidirectional path tracing. In *Compugraphics '93*, 95-104.

GEISLER, W.S. 1978. The effects of photopigment depletion on brightness and threshold. *Vision Res*., 18, 269-278.

GEISLER, W.S. 1979. Evidence for the equivalent background hypothesis in cones. *Vision Res*., 19, 799-805.

GLASSNER, A. S. 1989. *An introduction to ray tracing*, Academic Press Inc.

GLASSNER, S. A. 1995. *Principles of digital image synthesis*. Morgan Kauffman Publishers, Inc. ISBN 1-55860-276-3.

GROELLER, E. 1995. Nonlinear ray tracing: visualizing strange worlds*, Visual Computer 11(5), Springer Verlag*, *1995*, 263-274

MINNAERT, M.G.J. 1993. Light and color in the outdoors, *Springer-Verlag 1993*.

MUSGRAVE, F. K. 1990. A note on ray tracing mirages, *IEEE Computer Graphics and Applications, 10(6)*, 1990, 10-12.

MUSGRAVE , F. K. 1993. *Methods for realistic landscape rendering*, PhD. Thesis, Yale University.

NISHITA ,T. 1998. Light scattering models for the realistic rendering of natural scenes, *Proceedings of rendering Techniques '98*, 1-10.

PATTANAIK, S.N., TUMBLIN, J., YEE, H. and GREENBERG, D.P. 2000. Time-dependent visual adaptation for fast realistic image display. In *ACM Proceedings 2000*. ACM Press, 2000.

PREETHAM, A.J. 2003 Modeling Skylight and Aerial Perspective. *ATI Research, ACM SIGGRAPH 2003*

RUSHTON, W.A.H. 1963. The density of chlorolabale in the foveal cones of a protanope. *Journal of Physiology'63*, 168, 360-373.

RUSHTON, W.A.H. 1965. Cone pigment kinetics in the deuteranope. *Journal of Physiology'65*, London, 176, 38-45.

RUSHTON, W.A.H. 1972. Pigments and signals in colour vision. In *Journal of Physiology'72*, London, 220, 1-21P.

RUSHTON , W.A.H. and HENRY, G.H.. 1968. Bleaching and regeneration of cone pigments in man. *Vision Research 8*, 617-631.

SERÓN, F.J., GUTIÉRREZ, D., GUTIÉRREZ, G. and CEREZO, E. 2002. An implementation of a curved ray tracer for inhomogeneous atmospheres. In *ACM Transactions on Graphics, 2002.*

SMITH,V.C., POKORNY, J. and DIDDIE, K.R. 1988. Color matching and the Stiles-Crawford effect in observers with early age-related macular changes. *Journal of the Optical Society of America* A, Volume 5, Issue 12, 2113-December 1988.

SPERLING, H.G. 1986. Intense spectral light induced cone specific lesions of the retina and the effects of anesthesia. In *Hazards of Light eds. Cronly-Dillon*, J.R. et al., pp. 153-167. Oxford: Pergamon.

STAM , J. and LANGUENOU, E. 1996. Ray tracing in non-constant media. In *Proceedings of Rendering Techniques '96*, 225-234

VAN DER WERF, S. Y., GÜNTHER, G. P. and LEHN, W. H. 2003. Novaya Zemlya effects and sunsets. *Applied Optics, Vol. 42, No. 3, 20-1-2003*

VEACH , E. and GUIBAS, L. 1994. Bidirectional estimators for light transport. In *Fifth Eurographics Workshop on Rendering, 1994*, 147-162.

WALRAVEN, J. 1981. Perceived colour under conditions of chromatic adaptation: evidence for gain control by mechanisms. *Vision Res*., 21, 611-630.

WARD, G., RUSHMEIER, H. and PIATKO, C. 1997. A visibility matching tone reproduction operator for high dynamic range scenes. *IEEE Transactions on Visualization and Computer Graphics*, 3(4), pp. 291-306. October-November 1997

http://webvision.med.utah.edu

WYSZECKI, G. and STILES, W.S. 1982. *Color Science: Concepts and Methods, Quantitative Data and Formulae*. John Wiley and Sons, 2 edition.

YOUNG, A.T. 2000. Visualizing sunsets III. Visual adaptation and green flashes, *Journal of the Optical Society of America* A, vol. 17, pp. 2129-2139. December 2000